

# Theory of magnetic enhancement in strontium hexaferrite through Zn-Sn pair substitution

Laalitha S. I. Liyanage

*Department of Physics and Astronomy, Mississippi State University, Mississippi State, MS 39762, USA and  
Center for Advanced Vehicular Systems, Mississippi State University, Mississippi State, MS 39762, USA*

Sungho Kim

*Center for Computational Sciences, Mississippi State University, Mississippi State, MS 39762, USA*

Yang-Ki Hong and Ji-Hoon Park

*Department of Electrical and Computer Engineering and MINT Center,  
The University of Alabama, Tuscaloosa, AL 35487*

Steven C. Erwin

*Center for Computational Materials Science, Naval Research Laboratory, Washington, D.C. 20375, USA*

Seong-Gon Kim\*

*Department of Physics and Astronomy, Mississippi State University, Mississippi State, MS 39762, USA and  
Center for Computational Sciences, Mississippi State University, Mississippi State, MS 39762, USA*

(Dated: June 17, 2018)

We study the site occupancy and magnetic properties of Zn-Sn substituted  $M$ -type Sr-hexaferrite  $\text{SrFe}_{12-x}(\text{Zn}_{0.5}\text{Sn}_{0.5})_x\text{O}_{19}$  with  $x = 1$  using first-principles total-energy calculations. We find that in the lowest-energy configuration  $\text{Zn}^{2+}$  and  $\text{Sn}^{4+}$  ions preferentially occupy the  $4f_1$  and  $4f_2$  sites, respectively, in contrast to the model previously suggested by Ghasemi et al. [J. Appl. Phys., **107**, 09A734 (2010)], where  $\text{Zn}^{2+}$  and  $\text{Sn}^{4+}$  ions occupy the  $2b$  and  $4f_2$  sites. Density-functional theory calculations show that our model has a lower total energy by more than 0.2 eV per unit cell compared to Ghasemi's model. More importantly, the latter does not show an increase in saturation magnetization ( $M_s$ ) compared to the pure  $M$ -type Sr-hexaferrite, in disagreement with the experiment. On the other hand, our model correctly predicts a rapid increase in  $M_s$  as well as a decrease in magnetic anisotropy compared to the pure  $M$ -type Sr-hexaferrite, consistent with experimental measurements.

Keywords: Site preference; Hexaferrite; Magnetic property

## I. INTRODUCTION

Strontium hexaferrite  $\text{SrFe}_{12}\text{O}_{19}$  (SFO) is widely used as a material for permanent magnets, along with other  $M$ -type hexaferrites  $X\text{Fe}_{12}\text{O}_{19}$  ( $X = \text{Sr}, \text{Ba}, \text{Pb}$ ), due to their high Curie temperatures, large saturation magnetization, high coercivity, excellent chemical stability and low cost.<sup>1-3</sup> As shown in Fig. 1, magnetism in SFO results from  $\text{Fe}^{3+}$  ions occupying five crystallographically inequivalent sites in the unit cell: three octahedral sites ( $2a$ ,  $12k$ , and  $4f_2$ ), one tetrahedral site ( $4f_1$ ), and one trigonal bipyramid site ( $2b$ ). SFO is a ferrimagnetic material that has 16  $\text{Fe}^{3+}$  ions with spins in the majority direction ( $2a$ ,  $2b$ , and  $12k$  sites) and 8  $\text{Fe}^{3+}$  ions with spins in the minority direction ( $4f_1$  and  $4f_2$  sites) as shown in Fig. 1(c). Therefore, the substitution of non-magnetic ions into Fe sites with the minority spin direction has the potential to increase the saturation magnetization of SFO by reducing the negative contribution toward the saturation magnetization ( $M_s$ ). Consequently, investigations to improve the magnetic prop-

erties of  $M$ -type hexaferrites have been made using various nonmagnetic impurities.<sup>1-19</sup> Zr-Cd substituted SFO ( $\text{SrFe}_{12-x}(\text{Zr}_{0.5}\text{Cd}_{0.5})_x\text{O}_{19}$ ) showed an increase of  $M_s$  up to  $x = 0.2$ , while the coercivity decreased continuously with increasing Zr-Cd concentration.<sup>10</sup> For Er-Ni substituted SFO,  $M_s$  and coercivity steadily increased with Er-Ni concentration.<sup>3</sup> Substitution by Zn-Nb<sup>18</sup>, Zn-Sn<sup>6,20</sup> and Sn-Mg<sup>2</sup> increased  $M_s$  and decreased coercivity. These results call for a systematic understanding, from first principles, of why certain combinations of dopants lead to particular results. This theoretical understanding will open the door to systematically optimizing the properties of SFO.

There have been several previous first-principles investigations of SFO. Fang et al. investigated the electronic structure of SFO using density-functional theory (DFT).<sup>21</sup> Novak et al. calculated the electronic structure and exchange interactions of barium hexaferrite using DFT.<sup>22</sup> In spite of the importance of substituted SFO, only a few theoretical investigations have been done, and have focused on La substitution.<sup>23,24</sup> To our knowledge, no electronic structure calculation has been done on Zn-Sn-substituted SFO.

In this work we use first-principles total-energy calculations to study the site preference and mag-

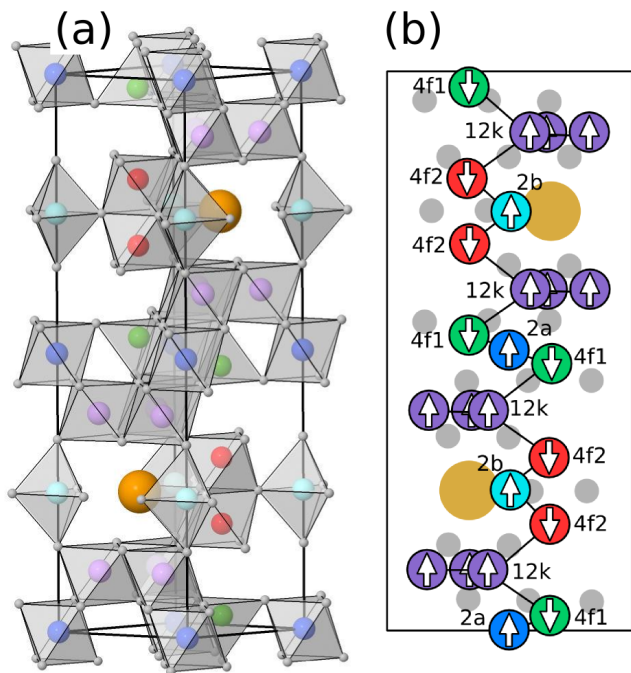


FIG. 1. (Color online) (a) One double formula unit cell of  $\text{SrFe}_{12}\text{O}_{19}$ . Two large gold spheres are Sr atoms and small gray spheres are O atoms. Colored spheres enclosed by polyhedra formed by O atoms represent  $\text{Fe}^{3+}$  ions in different inequivalent sites: 2a (blue), 2b (cyan), 12k (purple),  $4f_1$  (green), and  $4f_2$  (red). (b) A schematic diagram of the lowest-energy spin configuration of  $\text{Fe}^{3+}$  ions of  $\text{SrFe}_{12}\text{O}_{19}$ . The arrows represent the local magnetic moment at each atomic site.

netic properties of Zn-Sn substituted *M*-type SFO  $\text{SrFe}_{12-x}(\text{Zn}_{0.5}\text{Sn}_{0.5})_x\text{O}_{19}$  with  $x = 1$ . Based on total energy calculations, we conclude that in the ground-state configuration Zn and Sn ions preferentially occupy  $4f_1$  and  $4f_2$  sites, respectively. This is different from the model suggested by Ghasemi and co-workers<sup>6,20</sup>, where Zn and Sn ions occupy 2b and  $4f_2$  sites, respectively. We further show that our model predicts an increase of saturation magnetization as well as a decrease in magnetic anisotropy energy (MAE) compared to the pure *M*-type SFO ( $x = 0$ ) consistent with experimental observations.

## II. METHODS

To determine the site preference of Zn and Sn atoms in Sr-hexaferrite, we use first-principles total-energy calculations for configurations of  $\text{SrFe}_{12-x}(\text{Zn}_{0.5}\text{Sn}_{0.5})_x\text{O}_{19}$  at  $x = 0$  and  $x = 1$ . We used a unit cell which contains two formula units of SFO. The  $x = 1$  configuration was constructed by substituting Zn and Sn, one atom each, into the Fe sublattices of SFO. Total energies and forces were calculated using density-functional theory (DFT) with projector augmented wave (PAW) potentials as implemented in VASP.<sup>25,26</sup> All calculations were spin polar-

ized according to the ferrimagnetic ordering of Fe spins as shown in Fig. 1(b) as first proposed by Gorter.<sup>21,27</sup> A plane-wave energy cutoff of 520 eV was used for pure SFO and 400 eV for  $\text{SrFe}_{12-x}(\text{Zn}_{0.5}\text{Sn}_{0.5})_x\text{O}_{19}$  with  $x = 1$ . Reciprocal space was sampled with a  $7 \times 7 \times 1$  Monkhorst-Pack mesh<sup>28</sup> with a Fermi-level smearing of 0.2 eV applied through the Methfessel-Paxton method<sup>29</sup> for relaxations and the tetrahedron method<sup>30</sup> for static calculations. We performed geometric optimizations to relax the positions of ions and cell shape until the largest force component on any ion was less than 0.01 eV/Å. Electron exchange and correlation were treated with the generalized gradient approximation (GGA) as parameterized by the Perdew-Burke-Ernzerhof (PBE) scheme.<sup>31</sup>

To improve the description of localized Fe 3d electrons, we employed the GGA+U method in the simplified rotationally invariant approach described by Dudarev et al..<sup>32</sup> The method requires an effective  $U$  value ( $U_{\text{eff}}$ ) equal to the difference between the Hubbard parameter  $U$  and the exchange parameter  $J$ . The effective  $U$  (simply  $U$  from now on) parameter can be determined in a number of ways so as to reproduce various experimental or theoretical results of particular interest. Here we choose the value of  $U$  that best reproduces the local magnetic moments of the Fe ions obtained from a more rigorous calculation using the hybrid functional of Heyd, Scuseria, and Ernzerhof (HSE).<sup>33–35</sup> Thus our computational approach consisted of the following sequence. (1) Use PBE to optimize the volume and internal coordinates of pure SFO. (2) Use HSE to determine the individual Fe local moments of pure SFO. (3) Within GGA+U, determine the value of  $U$  that best reproduces the HSE local moments. (4) Use GGA+U to investigate the effects of varying the sites on which Zn and Sn substitute for Fe.

## III. RESULTS

### A. Pure $\text{SrFe}_{12}\text{O}_{19}$

Pure SFO ( $\text{SrFe}_{12-x}(\text{Zn}_{0.5}\text{Sn}_{0.5})_x\text{O}_{19}$  with  $x = 0$ ) has the hexagonal crystal structure and the space group  $P6_3/mmc$  as shown in Fig. 1. As shown in Table I, the unit cell has 11 inequivalent sites: one Sr site of multiplicity 2, five Fe sites of multiplicity 2, 2, 4, 4 and 12, and five oxygen sites of multiplicity 4, 4, 6, 12, and 12. In total the double formula unit cell has 64 atomic sites. Our DFT calculations showed that the spins of  $\text{Fe}^{3+}$  ions on these sites are arranged in an alternating fashion shown in Fig. 1(b) as first proposed by Gorter.<sup>21,27</sup> This antiferromagnetic arrangement of the spins of  $\text{Fe}^{3+}$  ions in the neighboring layers is consistent with the positive values of the dominant intersublattice exchange integrals of  $\text{SrFe}_{12}\text{O}_{19}$ <sup>36</sup> and closely related  $\text{BaFe}_{12}\text{O}_{19}$ <sup>22</sup>. DFT calculations showed that deviation from this configuration always costs energy.<sup>21,36</sup> Therefore, we set the initial spin direction of  $\text{Fe}^{3+}$  ions as Fig. 1(b) for all subsequent calculations.

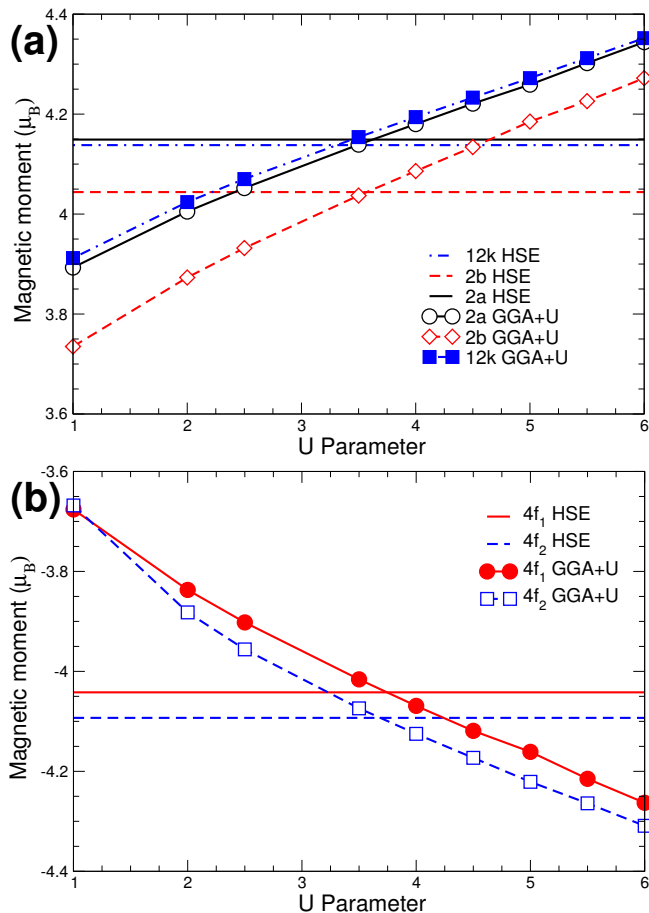


FIG. 2. (Color online) Variation of local magnetic moments of the five inequivalent Fe sites of SFO with respect to the  $U$  parameter; (a) positive magnetic moments for 2a, 2b, and 12k sites and (b) negative magnetic moments for 4f<sub>1</sub> and 4f<sub>2</sub> sites. Values from HSE are shown as horizontal lines.

The dependence of the local magnetic moments of Fe<sup>+3</sup> ions on the parameter  $U$  is plotted in Fig. 2. The local magnetic moments were computed using the PAW projector functions. Values from the HSE calculations are also shown as horizontal lines for comparison. The local magnetic moments vary monotonically over the range of  $U$  values and, more importantly, they cross their corresponding values of HSE calculation *simultaneously* near  $U = 3.7$  eV. Therefore, we set  $U$  to this value for all subsequent calculations. This value is between the two values,  $U = 3.4$  eV and  $U = 6.9$  eV, chosen by Novak et al. for their GGA+U calculations of Ba-hexaferrites with the full potential linearized augmented plane wave (FPLAPW) method<sup>22</sup>, and hence is quite reasonable.

For the optimized crystal structure we obtained the lattice constants  $a = 5.93$  Å and  $c = 23.20$  Å in good agreement with the experimental values of 5.88 Å and 23.04 Å, respectively.<sup>37</sup> The total densities of states (DOS) for SFO calculated with GGA ( $U = 0$ ), GGA+U and HSE are shown in Fig. 3. HSE and GGA+U correctly predict an insulating state while GGA predicts a metallic state.

TABLE I. Local magnetic moment of atoms in different inequivalent sites of SFO calculated using GGA ( $U = 0$ ), GGA+U ( $U = 3.7$  eV), and HSE functionals. Total magnetic moment ( $m_{\text{tot}}$ ) of the unit cell is also given. All moments are given in  $\mu_B$ .

site	GGA	GGA+U	HSE
Sr (2d)	-0.005	-0.003	-0.008
Fe (2a)	3.733	4.156	4.149
Fe (2b)	3.541	4.057	4.044
Fe (4f <sub>1</sub> )	-3.426	-4.038	-4.042
Fe (4f <sub>2</sub> )	-3.166	-4.095	-4.093
Fe (12k)	3.719	4.170	4.138
O (4e)	0.383	0.353	0.391
O (4f)	0.121	0.089	0.093
O (6h)	0.085	0.027	0.031
O (12k)	0.093	0.084	0.082
O (12k)	0.175	0.180	0.196
$m_{\text{tot}}$	40	40	40

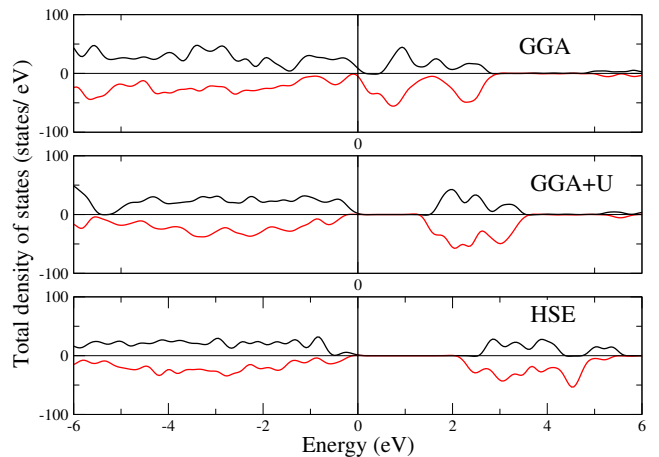


FIG. 3. (Color online) Total densities of states (DOS) of SrFe<sub>12</sub>O<sub>19</sub> calculated using GGA, GGA+U ( $U = 3.7$  eV), and HSE. Band gaps are 0.93 and 1.19 eV for GGA+U and HSE, respectively. Positive (negative) values correspond to majority (minority) spin states.

The local magnetic moments of the 11 inequivalent Fe sites and the total magnetic moment are given in Table I. Local magnetic moments of the Fe sites predicted by GGA are much less than those by HSE. GGA+U's prediction of the local magnetic moments is in good agreement with HSE's results. The total magnetic moment values are 40  $\mu_B$  per unit cell for all three methods.

### B. SrFe<sub>12-x</sub>(Zn<sub>0.5</sub>Sn<sub>0.5</sub>)<sub>x</sub>O<sub>19</sub> with $x = 1$

For  $x = 1$ , one Zn and one Sn atom are substituted at two of the 24 Fe sites of unit cell as shown in Fig. 4. All Fe sublattices listed in Table I have more than one equivalent atomic site. Substitution of Zn-Sn atoms breaks the symmetry of the equivalent sites of pure SFO. Out

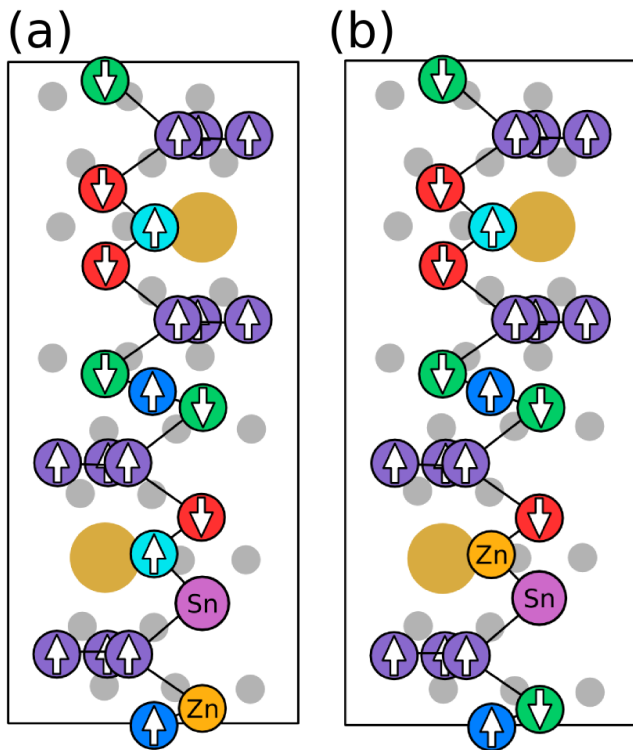


FIG. 4. (Color online) The structures of  $\text{SrFe}_{12-x}(\text{Zn}_{0.5}\text{Sn}_{0.5})_x\text{O}_{19}$  with  $x = 1$  with spins oriented in easy axis (001): (a) Our proposed ground state configuration  $\text{Zn}(4f_1)\text{Sn}(4f_2).1$  and (b) Ghasemi's proposed configuration  $\text{Zn}(2b)\text{Sn}(4f_2).1$ , which has higher total energy. Zn and Sn atoms are labeled. Other atoms are colored as in Fig. 1.

of all 552 ( $= 24 \times 23$ ) possible structures, the 24 symmetry operations of the space group  $P6_3/mmc$  leave a total of 55 inequivalent structures. We label these inequivalent configurations using the convention of Zn(site for Zn)Sn(site for Sn).(unique index). For example, when Zn and Sn are substituted at the  $2b$  and  $12k$  sites, respectively, there are 24 ( $= 12 \times 2$ ) possible structures but only two of them are inequivalent. Therefore, they are labeled as  $\text{Zn}(2b)\text{Sn}(12k).1$  and  $\text{Zn}(2b)\text{Sn}(12k).2$ . These structures were constructed by substituting Zn and Sn atoms to the respective sites of a SFO unit cell and optimizing all atomic positions using GGA+U.

Table II lists the nine lowest energy configurations. The lowest-energy configuration  $\text{Zn}(4f_1)\text{Sn}(4f_2).1$  (Fig. 4(a)) has Zn and Sn atoms substituted at the  $4f_1$  and  $4f_2$  sites, respectively, and shows an increase of  $10 \mu_B$  per unit cell in  $m_{\text{tot}}$  with respect to pure SFO consistent with the experimental results of Ghasemi and co-workers.<sup>6,20</sup> On the other hand, the structure suggested by Ghasemi with  $\text{Zn}^{2+}$  in  $2b$  site and  $\text{Sn}^{4+}$  in  $4f_2$  site (configuration  $\text{Zn}(2b)\text{Sn}(4f_2).1$  in Table II and shown in Fig. 4(b)) is energetically less favorable by 0.211 eV. Furthermore, this configuration shows no increase in  $m_{\text{tot}}$  contradicting the experimental result that showed a rapid

TABLE II. Nine lowest energy configurations of  $\text{SrFe}_{12-x}(\text{Zn}_{0.5}\text{Sn}_{0.5})_x\text{O}_{19}$  for  $x = 1$ . Total energies ( $E_{\text{tot}}$ ) are relative to that of the ground state configuration  $\text{Zn}(4f_1)\text{Sn}(4f_2).1$ . The total magnetic moment ( $m_{\text{tot}}$ ) and its change with respect to pure SFO ( $\Delta m_{\text{tot}}$ ) are also given. All values are for a double formula unit cell containing 64 atoms.

rank	configuration	$E_{\text{tot}}$ (eV)	$m_{\text{tot}}$ ( $\mu_B$ )	$\Delta m_{\text{tot}}$ ( $\mu_B$ )
1	$\text{Zn}(4f_1)\text{Sn}(4f_2).1$	0.000	50	10
2	$\text{Zn}(4f_1)\text{Sn}(4f_2).2$	0.133	50	10
3	$\text{Zn}(12k)\text{Sn}(4f_2).1$	0.170	40	0
4	$\text{Zn}(4f_1)\text{Sn}(12k).1$	0.188	40	0
5	$\text{Zn}(4f_1)\text{Sn}(4f_2).3$	0.192	50	10
6	$\text{Zn}(2b)\text{Sn}(4f_2).1$	0.211	40	0
7	$\text{Zn}(4f_1)\text{Sn}(4f_2).4$	0.234	50	10
8	$\text{Zn}(4f_1)\text{Sn}(2a).1$	0.262	40	0
9	$\text{Zn}(2a)\text{Sn}(4f_2).1$	0.381	40	0

increase of saturation magnetization with concentration  $x$  ( $\sim 7\%$  increase at  $x = 1$ ). We note that configurations with Zn and Sn substituted at the  $4f_1$  and  $4f_2$  sites show a considerable increase in  $m_{\text{tot}}$  ( $= 10 \mu_B$ ) while those at the  $2a$ ,  $2b$ , and  $12k$  sites show zero increase.

In Table III we compare the contribution of different sublattices to the total magnetic moment in these two proposed models for the structure of  $\text{SrFe}_{12-x}(\text{Zn}_{0.5}\text{Sn}_{0.5})_x\text{O}_{19}$  with  $x = 1$ . To see the effect of Zn and Sn atoms in different sublattices, we split the entries of sublattices containing these atoms ( $4f_1$ ,  $4f_2$ , and  $2b$ ). As expected,  $\text{Zn}^{2+}$  and  $\text{Sn}^{4+}$  ions carry negligible magnetic moments regardless of their substitution sites. Consequently, when they replace  $\text{Fe}^{3+}$  ions in the minority spin sites ( $4f_1$  and  $4f_2$ ), they eliminate a negative contribution and hence increase the total magnetic moment per unit cell. On the other hand, when  $\text{Zn}^{2+}$  and  $\text{Sn}^{4+}$  ions replace  $\text{Fe}^{3+}$  ions in the majority spin site ( $2b$ ), they eliminate a positive contribution and hence reduce the total moment. Therefore, configuration  $\text{Zn}(4f_1)\text{Sn}(4f_2).1$  results in an increase of  $10 \mu_B$  per unit cell for the total magnetic moment  $m_{\text{tot}}$ , whereas configuration  $\text{Zn}(2b)\text{Sn}(4f_2).1$ , where Zn and Sn are substituted to the  $2b$  and  $4f_2$  sites, shows no increase in  $m_{\text{tot}}$  as the effect of Zn in the  $2b$  site cancels out that of Sn in the  $4f_2$  site.

In addition to an increase in the total magnetic moment, Ghasemi et al. also reported a rapid decrease in anisotropy of SFO due to Zn and Sn substitution.<sup>6</sup> This decrease was attributed to the substitution of  $\text{Zn}^{2+}$  ions on the  $2b$  site. We calculated the magnetic anisotropy energy (MAE) for the two models. A self-consistent calculation on the fully relaxed crystal structure was performed. Then non-self-consistent calculations were performed with the spin quantization axis oriented along the easy axis and the hard plane. MAE is the difference of total energies from these two calculations:

$$E_{\text{MAE}} = E_{(100)} - E_{(001)}$$

where  $E_{(100)}$  is the total energy with spin quantization

TABLE III. Contribution of atoms in each sublattice to the total magnetic moment of Zn-Sn-substituted SFO structures Zn( $4f_1$ )Sn( $4f_2$ ).1 and Zn( $2b$ )Sn( $4f_2$ ).1 compared with pure SFO. All moments are in  $\mu_B$ .  $\Delta m$  is measured relative to the values for pure SFO. Note that the total magnetic moment of the unit cell ( $m_{\text{tot}}$ ) is slightly different than the sum of local magnetic moments due to the contribution from the interstitial region.

site	SFO		Zn( $4f_1$ )Sn( $4f_2$ ).1			Zn( $2b$ )Sn( $4f_2$ ).1		
	atoms	$m$	atoms	$m$	$\Delta m$	atoms	$m$	$\Delta m$
$2d$	2 Sr	-0.01	2 Sr	0.00	0.00	2 Sr	0.00	0.00
$2a$	2 Fe	8.31	2 Fe	8.35	0.04	2 Fe	8.30	-0.01
$2b$	1 Fe	4.06	1 Fe	4.14	0.08	1 Fe	4.05	-0.01
	1 Fe	4.06	1 Fe	4.05	-0.01	1 <b>Zn</b>	-0.01	-4.07
$4f_1$	3 Fe	-12.11	3 Fe	-12.06	0.03	3 Fe	-12.07	0.04
	1 Fe	-4.04	1 <b>Zn</b>	0.06	4.10	1 Fe	-4.03	0.01
$4f_2$	3 Fe	-12.29	3 Fe	-12.25	0.04	3 Fe	-12.30	-0.02
	1 Fe	-4.10	1 <b>Sn</b>	0.06	4.16	1 <b>Sn</b>	0.04	4.14
$12k$	12 Fe	50.04	12 Fe	50.30	0.26	12 Fe	50.12	0.06
$4e$	4 O	1.41	4 O	1.43	0.02	4 O	1.41	0.00
$4f$	4 O	0.36	4 O	0.57	0.21	4 O	0.34	-0.02
$6h$	6 O	0.16	6 O	0.41	0.25	6 O	-0.11	-0.27
$12k$	12 O	1.00	12 O	1.62	0.62	12 O	1.04	0.04
$12k$	12 O	2.16	12 O	2.15	-0.01	12 O	2.35	0.19
$\sum m$		39.02		48.81	9.79		39.13	0.10
$m_{\text{tot}}$		40		50	10		40	0

TABLE IV. Magnetic anisotropy energy (MAE) and magnetic anisotropy constant  $K$  for pure SFO and two configurations of SrFe $_{12-x}$ (Zn $_{0.5}$ Sn $_{0.5}$ ) $_x$ O $_{19}$  with  $x = 1$ .

Configuration	MAE (meV)	$K$ (kJ·m $^{-3}$ )
SFO	0.84	190
Zn( $4f_1$ )Sn( $4f_2$ ).1	0.45	100
Zn( $2b$ )Sn( $4f_2$ ).1	0.53	120

axis in the hard direction and  $E_{(001)}$  the total energy with spin quantization axis in the easy direction. Using the MAE, the magnetic anisotropy constant  $K$  can be computed:

$$K = \frac{E_{\text{MAE}}}{V \sin^2 \theta}$$

where  $V$  is the equilibrium volume of the unit cell and  $\theta$  is the angle between the two spin quantization axis orientations ( $90^\circ$  in the present case). Results of these calculations are presented in Table IV, which shows that both models show a rapid decrease in anisotropy consistent with the experimental results.

#### IV. DISCUSSION

The present work reveals a new structural model for Zn-Sn-substituted SFO, Zn( $4f_1$ )Sn( $4f_2$ ).1, which is different from the previously proposed model, Zn( $2b$ )Sn( $4f_2$ ).1, by Ghasemi et al.<sup>6,20</sup> Three independent results support this new model:

1. Energy: The new model has a significantly lower

total energy per Zn-Sn pair, by 0.211 eV, compared to Ghasemi's model.

2. Magnetization: The new model exhibit an increase of 10  $\mu_B$  in total magnetic moment consistent with the experiment. In contrast, Ghasemi's model shows no increase in total magnetic moment as Zn atoms in the  $2b$  site cancel the contribution of Sn atoms in the  $4f_2$  site.

3. Anisotropy: Both models are compatible with the experimental observation of rapid decrease in magnetic anisotropy energy.

Ghasemi's model and our model agree on the site for Sn atoms ( $4f_2$ ), but differ on the site for Zn atoms ( $4f_1$  for the present model and  $2b$  for Ghasemi's). To understand the source of this discrepancy, we briefly review the reasoning behind Ghasemi's model.

Ghasemi and co-workers proposed their model on the basis of Mössbauer spectroscopy and magnetic anisotropy data. The measured  $^{57}\text{Fe}$  Mössbauer spectrum of SrFe $_{12-x}$ (Zn $_{0.5}$ Sn $_{0.5}$ ) $_x$ O $_{19}$  was fitted by a superposition of five magnetically split components (sextets) corresponding to the  $2a$ ,  $2b$ ,  $4f_1$ ,  $4f_2$ , and  $12k$  sites. The relative intensity ratio of the five sextets were adjusted to obtain a satisfactory fit to the measured spectrum. The resultant ratios correspond to the occupancy of Fe $^{+3}$  ions in each site. For pure SFO, the intensity ratios corresponding to the  $2a$ ,  $2b$ ,  $4f_1$ ,  $4f_2$ , and  $12k$  sites would have been 1:1:2:2:6. For SrFe $_{12-x}$ (Zn $_{0.5}$ Sn $_{0.5}$ ) $_x$ O $_{19}$  Ghasemi et al. obtained fitted intensity ratios 1:0:2:1:6, meaning that the Fe in the  $2b$  and  $4f_2$  sites were replaced by Zn and Sn. The assignment of Zn to the  $2b$  site was made by analogy to behavior in the related systems BaFe $_{12-x}$ (Zr $_{0.5}$ Zn $_{0.5}$ ) $_x$ O $_{19}$  and LaZnFe $_{11}$ O $_{19}$ .<sup>38,39</sup>

TABLE V. Relative total energy and magnetic moment of SFO when Zn or Sn atoms are substituted into Fe sites separately. Total energies ( $E_{\text{tot}}$ ) are relative to the lowest energy for each case. The total magnetic moment ( $m_{\text{tot}}$ ) and its change with respect to the pure SFO ( $\Delta m_{\text{tot}}$ ) are also given. All values are for a double formula unit cell containing 64 atoms.

atom	site	$E_{\text{tot}}$ (eV)	$m_{\text{tot}}$ ( $\mu_B$ )	$\Delta m_{\text{tot}}$ ( $\mu_B$ )
Zn	$4f_1$	0.000	45	+5
Zn	$2a$	0.312	35	-5
Zn	$12k$	0.367	35	-5
Zn	$2b$	0.821	35	-5
Zn	$4f_2$	1.073	45	+5
Sn	$4f_2$	0.000	43	+3
Sn	$2b$	0.055	33	-7
Sn	$12k$	0.222	33	-7
Sn	$2a$	0.462	33	-7
Sn	$4f_1$	0.770	43	+3

One possible source of the discrepancy between two models is that the interpretation of Mössbauer spectra is not straightforward.<sup>20</sup> Competing sets of intensity ratios may produce fits of similar qualities. It would be interesting to see if a re-fitting based on our present model would reproduce the Mössbauer spectrum.

To further elucidate the stability of  $\text{Zn}(4f_1)\text{Sn}(4f_2)_2$  for Zn-Sn-substituted SFO, we investigated the site preference of Zn and Sn atoms separately. Table V shows the relative total energies and magnetic moment of SFO when Zn or Sn atoms are substituted into Fe sites separately. Our result shows that Zn prefers  $4f_1$  site while Sn prefers  $4f_2$  site even when they are substituted separately. These preferences can be also understood in terms of the oxidation states of all the ions. The tetrahedral  $4f_1$  site is enclosed by four O atoms (three  $12k$ -O and one  $4f$ -O). Each of these O atoms is shared by four other Fe sites. Since O ions have a  $-2$  oxidation state, we can assign  $-2$  [ $= 4(1/4)(-2)$ ] as the oxidation state of the  $4f_1$  site and conclude that the  $4f_1$  site will prefer to host ions with a  $+2$  oxidation state such as  $\text{Zn}^{+2}$ . Similarly, the octahedral  $4f_2$  site is enclosed by six O atoms (three  $12k$ -O and three  $6h$ -O). Each of these O atoms is shared by three other Fe sites. Thus, we can assign  $-4$  [ $= 6(1/3)(-2)$ ] as the oxidation state of the  $4f_2$  site and

conclude that the  $4f_2$  site will prefer to host ions with a  $+4$  oxidation state such as  $\text{Sn}^{+4}$ . On the other hand, the hexahedral (trigonal bipyramidal)  $2b$  site is enclosed by five O atoms: three  $6h$ -O atoms are shared by three other Fe sites while two  $4e$ -O atoms by four other Fe sites. Thus, we can assign  $-3$  [ $= 3(1/3)(-2) + 2(1/4)(-2)$ ] as the oxidation state of the  $2b$  site and conclude that the  $2b$  site will prefer to host ions with a  $+3$  oxidation state such as  $\text{Fe}^{+3}$ . This analysis supports the site preference of the present model where  $\text{Zn}^{+2}$  and  $\text{Sn}^{+4}$  ions occupy  $4f_1$  and  $4f_2$  sites, respectively.

## V. CONCLUSION

Using first-principles total energy calculations based on density functional theory, we obtained the ground state structure for Zn-Sn-substituted SFO,  $\text{SrFe}_{12-x}(\text{Zn}_{0.5}\text{Sn}_{0.5})_x\text{O}_{19}$  with  $x = 1$ . We showed that  $\text{Zn}^{2+}$  and  $\text{Sn}^{4+}$  ions preferentially occupy  $4f_1$  and  $4f_2$  sites. The stable structure derived from our calculations shows a rapid increase in saturation magnetization and a significant decrease in magnetocrystalline anisotropy with respect to pure SFO that is consistent with experimental observations. We showed that the previously proposed model with Zn atom in the  $2b$  is a higher-energy configuration. We also showed that the lowest-energy configuration determined from the present work shows a rapid decrease in anisotropy consistent with the experimental results.

## VI. ACKNOWLEDGMENT

This work was supported in part by the U.S. Department of Energy ARPA-E REACT program under Award Number de-ar0000189, the Center for Advanced Vehicular Systems (CAVS), and the Center for Computational Science (CCS) at Mississippi State University. Funding for this project was also provided by the Office of Naval Research (ONR) through the Naval Research Laboratory's Basic Research Program. Computer time allocation has been provided by the High Performance Computing Collaboratory (HPC<sup>2</sup>) at Mississippi State University.

\* Author to whom correspondence should be addressed; kimsg@ccs.msstate.edu

<sup>1</sup> Z. Pang, X. Zhang, B. Ding, D. Bao, and B. Han, Journal of Alloys and Compounds **492**, 691 (2010).

<sup>2</sup> A. Davoodi and B. Hashemi, Journal of Alloys and Compounds **509**, 5893 (2011).

<sup>3</sup> M. N. Ashiq, M. J. Iqbal, M. Najam-ul Haq, P. Hernandez Gomez, and A. M. Qureshi, Journal of Magnetism and Magnetic Materials **324**, 15 (2012).

<sup>4</sup> G. Asghar and M. Anis-ur-Rehman, Journal of Alloys and Compounds **526**, 85 (2012).

<sup>5</sup> M. N. Ashiq, M. Javed Iqbal, and I. Hussain Gul, Journal of Magnetism and Magnetic Materials **323**, 259 (2011).

<sup>6</sup> A. Ghasemi, V. Šepelák, X. Liu, and A. Morisako, Journal of Applied Physics **107**, 09A734 (2010).

<sup>7</sup> M. J. Iqbal, M. N. Ashiq, and P. H. Gomez, Journal of Alloys and Compounds **478**, 736 (2009).

<sup>8</sup> P. Bercoff, C. Herme, and S. Jacobo, Journal of Magnetism and Magnetic Materials **321**, 2245 (2009).

- <sup>9</sup> T. Nga, N. Duong, and T. Hien, *Journal of Alloys and Compounds* **475**, 55 (2009).
- <sup>10</sup> M. N. Ashiq, M. J. Iqbal, and I. H. Gul, *Journal of Alloys and Compounds* **487**, 341 (2009).
- <sup>11</sup> M. J. Iqbal, M. N. Ashiq, P. Hernandez-Gomez, and J. M. Munoz, *Journal of Magnetism and Magnetic Materials* **320**, 881 (2008).
- <sup>12</sup> N. Rezlescu, C. Doroftei, E. Rezlescu, and P. Popa, *Journal of Alloys and Compounds* **451**, 492 (2008).
- <sup>13</sup> M. J. Iqbal, M. N. Ashiq, P. Hernandez-Gomez, and J. M. Munoz, *Scripta Materialia* **57**, 1093 (2007).
- <sup>14</sup> M. J. Iqbal and M. N. Ashiq, *Scripta Materialia* **56**, 145 (2007).
- <sup>15</sup> L. Qiao, L. You, J. Zheng, L. Jiang, and J. Sheng, *Journal of Magnetism and Magnetic Materials* **318**, 74 (2007).
- <sup>16</sup> Q. Fang, H. Cheng, K. Huang, J. Wang, R. Li, and Y. Jiao, *Journal of Magnetism and Magnetic Materials* **294**, 281 (2005).
- <sup>17</sup> J. Wang, C. Ponton, R. Grössinger, and I. Harris, *Journal of Alloys and Compounds* **369**, 170 (2004).
- <sup>18</sup> Q. Fang, *Journal of Applied Physics* **95**, 6360 (2004).
- <sup>19</sup> Q. Fang, W. Zhong, Z. Jin, and Y. Du, *Journal of Applied Physics* **85**, 1667 (1999).
- <sup>20</sup> A. Ghasemi and V. Šepelák, *Journal of Magnetism and Magnetic Materials* **323**, 1727 (2011).
- <sup>21</sup> C. Fang, F. Kools, R. Metselaar, R. Groot, and Others, *Journal of Physics: Condensed Matter* **15**, 6229 (2003).
- <sup>22</sup> P. Novák and J. Ruzs, *Phys. Rev. B* **71**, 184433 (2005).
- <sup>23</sup> M. Küpferling, P. Novák, K. Knížek, M. W. Pieper, R. Grössinger, G. Wiesinger, and M. Reissner, *Journal of Applied Physics* **97**, 10F309 (2005).
- <sup>24</sup> P. Novk, K. Knek, M. Kpferling, R. Grssinger, and M. W. Pieper, *The European Physical Journal B - Condensed Matter and Complex Systems* **43**, 509 (2005), 10.1140/epjb/e2005-00084-8.
- <sup>25</sup> G. Kresse and J. Furthmüller, *Phys. Rev. B* **54**, 11169 (1996).
- <sup>26</sup> G. Kresse and D. Joubert, *Phys. Rev. B* **59**, 1758 (1999).
- <sup>27</sup> E. F. Gorter, *Proc. IEEE* **104B**, 2555 (1957).
- <sup>28</sup> H. Monkhorst and J. Pack, *Phys. Rev. B* **13**, 5188 (1976).
- <sup>29</sup> M. Methfessel and A. T. Paxton, *Phys. Rev. B* **40**, 3616 (1989).
- <sup>30</sup> P. E. Blöchl, O. Jepsen, and O. K. Andersen, *Phys. Rev. B* **49**, 16223 (1994).
- <sup>31</sup> J. P. Perdew, K. Burke, and M. Ernzerhof, *Phys. Rev. Lett.* **77**, 3865 (1996).
- <sup>32</sup> S. L. Dudarev, G. A. Botton, S. Y. Savrasov, C. J. Humphreys, and A. P. Sutton, *Phys. Rev. B* **57**, 1505 (1998).
- <sup>33</sup> J. Heyd, G. E. Scuseria, and M. Ernzerhof, *The Journal of Chemical Physics* **118**, 8207 (2003).
- <sup>34</sup> J. Heyd and G. E. Scuseria, *The Journal of Chemical Physics* **121**, 1187 (2004).
- <sup>35</sup> J. Heyd, G. E. Scuseria, and M. Ernzerhof, *The Journal of Chemical Physics* **124**, 219906 (2006).
- <sup>36</sup> Laalitha S. I. Liyanage, Sungho Kim, Ji-Hoon Park, Yang-Ki Hong, Steven C. Erwin, and Seong-Gon Kim, (unpublished).
- <sup>37</sup> K. Kimura, M. Ohgaki, K. Tanaka, H. Morikawa, and F. Marumo, *Journal of Solid State Chemistry* **87**, 186 (1990).
- <sup>38</sup> Z. W. Li, C. K. Ong, Z. Yang, F. L. Wei, X. Z. Zhou, J. H. Zhao, and A. H. Morrish, *Phys. Rev. B* **62**, 6530 (2000).
- <sup>39</sup> X. Obradors, A. Collomb, M. Pernet, D. Samaras, and J. Joubert, *Journal of Solid State Chemistry* **56**, 171 (1985).